RSC Advances

This is an *Accepted Manuscript*, which has been through the Royal Society of Chemistry peer review process and has been accepted for publication.

Accepted Manuscripts are published online shortly after acceptance, before technical editing, formatting and proof reading. Using this free service, authors can make their results available to the community, in citable form, before we publish the edited article. This *Accepted Manuscript* will be replaced by the edited, formatted and paginated article as soon as this is available.

You can find more information about *Accepted Manuscripts* in the Information for Authors.

Please note that technical editing may introduce minor changes to the text and/or graphics, which may alter content. The journal's standard Terms & Conditions and the Ethical guidelines still apply. In no event shall the Royal Society of Chemistry be held responsible for any errors or omissions in this *Accepted Manuscript* or any consequences arising from the use of any information it contains.

ROYAL SOCIETY OF CHEMISTRY

www.rsc.org/advances

Please do not adjust margins

RSC Advances

COMMUNICATION

Fuel Cell Anode Catalyst Performance can be Stabilized with a Molecularly Rigid Film of Polymer of Intrinsic Microporosity (PIM)

Received 00th January 20xx,
Accepted 00th January 20xx

DOI: 10.1039/x0xx00000x

www.rsc.org/

Daping He [a], Yuanyang Rong [a], Mariolino Carta [b], Richard Malpass-Evans [b], Neil B. McKeown [b], and Frank Marken [a]*

There remains a major materials challenge in maintaining the performance of platinium (Pt) anode catalysts in fuel cells due to corrosion and blocking of active sites. Herein, we report a new materials strategy for improving anode catalyst stability based on a protective microporous coating with an inert and highly rigid (non-blocking) polymer of intrinsic microporosity (PIM-EA-TB). The "anti-corrosion" effect of the PIM-EA-TB coating is demonstrated with a commercial Pt catalyst (3-5 nm diameter, 40 wt% Pt on Vulcan-72) and for three important fuel cell anode reactions: (i) methanol oxidation, (ii) ethanol oxidation, and (iii) formic acid oxidation.

Fuel cells powered by oxidation of small organic molecules (such as methanol, ethanol, formic acid, etc.) can be highly efficient, environmentally friendly, convenient in terms of fuel storage and infrastructure, and relatively simple in terms of device manufacturing.[1-4] A significant challenge remaining in the large-scale implementation of low temperature fuel cells (such as polymer-electrolyte or PEM fuel cells for cars) is the often rapid degradation of catalysts (depending on operational conditions) in both anode and cathode compartments due to catalyst migration, Oswald ripening, carbon substrate corrosion, and loss of catalyst form the surface.[5,6] These losses are linked often to short operational bursts or switching during power generation. This leads to the irreversible decay of fuel performance associated with additional costs of maintenance.[1, 7-9] Conditions during operational deterioration of catalysts can be simulated by accelerated degradation testing (ADT) based on repeated potential cycles.

Due to the insufficient activity of non-noble metal catalysts, the most commonly used fuel cell catalysts to date are 3–5 nm diameter Pt nanoparticles, which are supported on commercial carbon supports such as Vulcan-72.[10,11] The well-known detrimental corrosion processes for Pt nanocatalysts include electro-corrosion via Pt dissolution and colloidal mobility, aggregation, and poisoning by intermediates and corrosion products during small organic fuel molecule oxidation.[12-14] A simple materials solution such as a protective coating is highly desirable.

Employing polymer functionalization to optimize the performance of commercial Pt/C catalysts and to design new nano-composite catalyst systems are both promising strategies for fuel cell catalyst development and engineering. Some advanced polymers, such as polyaniline (PANI)[13,15,16,17] or PTFE/perfluorosulfonic acid (PFSA)[18-20] have received special attention in fuel cell catalyst stabilization, because of their unique conductive and/or proton mobility properties. Interfacial Pt-catalyst engineering for example with pyridine-containing poly-benzimidazole on multi-walled carbon nanotubes has been reported to improve catalyst performance for methanol fuel cells.[21] These materials lead locally to high electrical and proton conductivity and good chemical stability in acidic environments. However, due to poor rigidity these materials also strongly interact with catalyst surfaces. Challenges are still considerable in precisely controlling the thickness of these solid polymer over-layers, which also increase the resistance towards reaction species transport to the catalyst surface and so detrimentally affect catalytic activity. A polymer with more rigid molecularly pre-defined microporosity could be a better alternative. The rigid structure of the polymer can maintain a permanent microporosity, which facilitates the transportation of the reaction species whilst suppressing morphological changes.

Recently, the novel class of intrinsically microporous polymer (PIM) materials has been developed primarily for a range of applications in gas membrane technology[22-26]. The structurally highly rigid PIM backbone achieves open packing to generate novel properties due to permanent microporosity. In our recent publications we have demonstrated benefits of PIM materials also in aqueous electrolyte media with potential applications emerging in electrochemical technology[27,28] and in

[a] Department of Chemistry, University of Bath, Claverton Down, Bath BA2 7AY, UK.
[b] School of Chemistry, University of Edinburgh, David Brewster Road,Edinburgh, EH9 3FJ, UK.

RSC Advances Accepted Manuscript

Please do not adjust margins

solution phase electrocatalysis.[29-32] Particularly useful is a novel amine-containing PIM (PIM-EA-TB), synthesised via a polymerisation reaction involving the formation of Tröger's base with high molecular mass (M_w>70,000 g mol^{-1}) and high BET surface area (1027 m^2 g^{-1}). This PIM material was shown to be applicable as an effective protection agent against Pt/C catalysts corrosion in fuel cell cathodes[32] (for oxygen reduction). In this report, it is demonstrated that the same methodology can be applied much more generally also for fuel cell anode catalysts in methanol, ethanol, or formic acid oxidation.

The rigid microporous PIM-EA-TB film is employed here as a coating to encapsulate the Pt/C catalysts (see Figure 1a) whilst maintaining effective diffusion channels of 1-3 nm diameter[26] for water and reaction species. The coating is applied on top of the catalyst composite layer by casting of a PIM-EA-TB solution in chloroform. A layer of 10 μg PIM-EA-TB is applied to a 6 mm diameter glassy carbon electrode with underlying catalyst to give a film of approximately 40 nm average thickness (or lower when taking into account surface roughness of the catalyst layer). The TEM image of commercial Pt/C catalyst (40 wt% on Vulcan-72) in Figure 1b shows a size range of 3 to 5 nm for Pt nanoparticles supported on carbon black. Figure 1c-d show SEM images of Pt/C (c) and PIM@Pt/C (d) catalysts. The PIM-EA-TB membrane layer was found distributed over catalyst layer surface (appearing as "haze" in the SEM image), which suggests a successful modification of the PIM-EA-TB film on top of the Pt/C catalyst.

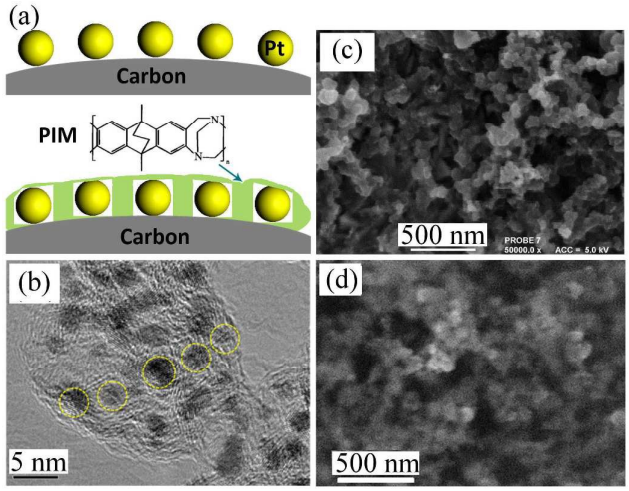

Fig. 1 (a) Schematic illustration of PIM-EA-TB rigidly encapulating and protecting Pt/C catalyst without blocking the surface. (b) TEM image of Pt/C catalyst. SEM images for Pt/C (c) and PIM@Pt/C (d) on glassy carbon electrode substrate.

Data in Figure 2a shows cyclic voltammetry responses for Pt/C (black) and for PIM@Pt/C (red) immersed in N_2-saturated 0.1 M $HClO_4$ at room temperature. Both voltammetric responses are dominated by the classic platinum surface signals and essentially identical. That is, under these conditions there is no direct effect of the PIM-EA-TB surface layer on these signals. The rigid molecular structure prevents blocking of surface sites on the platinum. The electrochemically active surface area (ESA) for the catalyst can be calculated from measuring the charge collected in the hydrogen adsorption/desorption region (see Q_H) and assuming 210 μC cm^{-2}.[33] Values obtained in this way are 53.4 m^2 g^{-1} for Pt/C and 52.5 m^2 g^{-1} for PIM@Pt/C. This provides strong evidence that only few surface Pt atoms are inactivated by bonding to the amine functionality within the PIM-EA-TB, which is due to the highly rigid and conformationally locked structure of the polymer.

Methanol electro-oxidation (which is important in direct methanol fuel cells[34]) was investigated in aqueous 0.1 M $HClO_4$ + 1 M CH_3OH as shown in Figure 2b. The process is known to yield predominantly carbon dioxide. The Pt/C and PIM@Pt/C catalysts show very similar onset potential and peak currents for methanol electro-oxidation, at least initially. Then, the long-term electrocatalytic stability for PIM@Pt/C and commercial Pt/C were tested by repeating the cyclic voltammetry potential sweeps for 200 cycles (see Figure 2c, d).

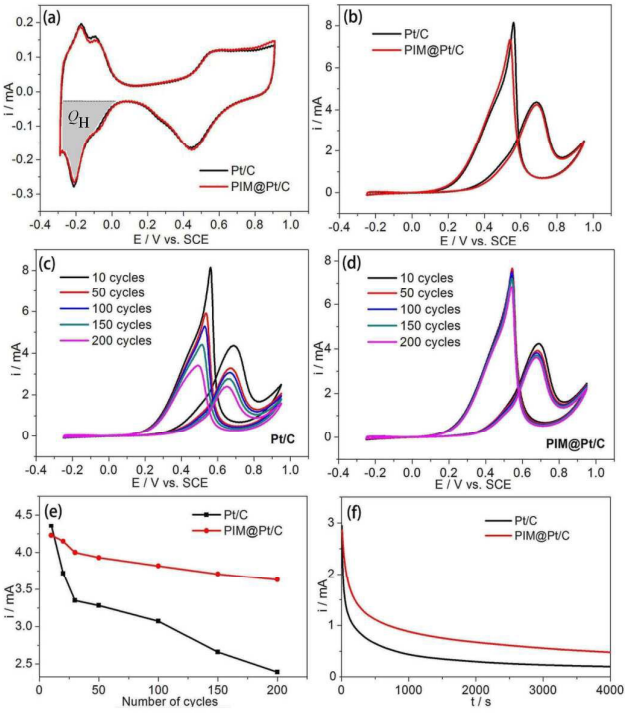

Fig. 2 (a) Cyclic voltammograms in N_2-saturated 0.1 M $HClO_4$ (50 mV s^{-1}) and (b) cyclic voltammograms for methonal oxidation in 0.1 M $HClO_4$ + 1 M CH_3OH for Pt/C and for PIM@Pt/C. (c,d) Cyclic voltammograms for Pt/C (c) and for PIM@Pt/C (d) showing accelerated degradation testing from -0.25 to +0.95 V vs. SCE. (e) Plot of electrocatalytic oxidation peaks for Pt/C and for PIM@Pt/C for the forward peak current for ethanol electro-oxidation over 200 cycles. (f) Chronoamperometric curves of Pt/C and PIM@Pt/ C at +0.6 V vs. SCE.

RSC Advances Accepted Manuscript

This journal is © The Royal Society of Chemistry 20xx

Whereas Pt/C catalyst (Figure 2c) suffers significant degradation and decay in the catalytic current (due to the harsh accelerated degradation conditions), the PIM@Pt/C catalyst (see Figure 2d) remains stable under these conditions. Figure 2e shows the normalized forward oxidation peak current versus the number of potential cycle for both catalysts, which demonstrates that the decrease of the forward peak current of PIM@Pt/C is much slower compared to that for the commercial unprotected Pt/C catalyst. After 200 potential cycles, 88% of the initial forward oxidation peak current was maintained for PIM@Pt/C as compared to only 48% for Pt/C. Additionally, chrono-amperometry test measurements were performed in aqueous 1 M methanol + 0.1 M $HClO_4$ at the oxidation potential of 0.6 V vs. SCE (see Figure 2f). After 4000 s, the current is 0.48 mA for PIM@Pt/C and only 0.21 mA for Pt/C – again indicative of enhanced catalyst stability during methanol oxidation. The results show significant benefits even at shorter times. This suggests that the polymer microporosity, in addition to enhancing durability due to corrosion protection, may help to maintain surface activity due to prevention of impurity adsorption and blocking.

Ethanol electro-oxidation (of interest for direct ethanol fuel cells[34]) was investigated under similar conditions (see Figure 3 a-d). Products for the process include carbon dioxde and acetic acid. Measurements are reported for PIM@Pt/C and Pt/C in the aqueous 0.1 M $HClO_4$ + 1 M ethanol at room temperature.

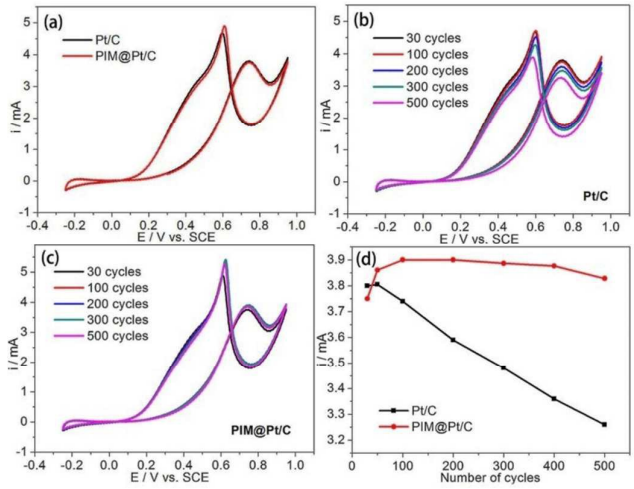

Fig. 3 (a) Cyclic voltammograms for ethanol oxidation recorded at room temperature in 0.1 M $HClO_4$ + 1 M CH_3CH_2OH (50 mVs^{-1}). (b,c) Cyclic voltammograms for Pt/C (c) and for PIM@Pt/C (d) for accelerated degradation testing from -0.25 to +0.95 V vs. SCE. (d) Plot of electrocatalytic peak currents of Pt/C and PIM@Pt/C referring to the forward peak current for ethanol electro-oxidation over 500 cycles.

Very similar cyclic voltammetry responses are obtained for ethanol electro-oxidation on both types of catalysts (Figure 3a). For the accelerated durability testing, cyclic voltammetry potential scans were performed for 500 continuous cycles. Figure 3b and 3c contrast the behaviour observed with/without the PIM-EA-TB film coating during durability testing. A significant decay in performance is seen only for the commercial Pt/C catalyst. Figure 3d shows the forward oxidation peak current density as a function of cyclic voltammetry scan number and demonstrates that the forward oxidation peak current density of PIM@Pt/C catalyst reaches the maximum (3.9 mA) at the 100th cycle, and then remains relatively constant. The initial increase could be linked to some relaxation in the polymer film. In contrast, a slow but monotonous decrease in catalyst performance with the number of potential cycle is seen on the commercial Pt/C catalyst. This behaviour is usually attributed to surface poisoning by CO-like species as well as the dissolution loss of Pt from the surface. After 500 potential cycles, 98% of the initial forward oxidation peak current was still maintained for PIM@Pt/C, as compared to the decrease to 85% of initial activity for Pt/C.

Formic acid electro-oxidation (for direct formic acid fuel cells[35]) activity was tested in aqueous 0.1 M $HClO_4$ + 1 M HCOOH (see Figure 4a). The process is known to lead to carbon dioxide as the principle product. Initially, both the Pt/C and the PIM@Pt/C catalysts show very comparable activities for formic acid electro-oxidation. The accelerated degradation testing by cyclic voltammetry and monitoring electrocatalytic performance for PIM@Pt/C and for commercial Pt/C are shown in Figure 4b and 4c. It can be seen that current peaks for commercial Pt/C catalyst (Figure 4b) change significantly, while the equivalent experiments with PIM@Pt/C (Figure 4c) demonstrate much greater robustness. The backward potential scan oxidation peak drops dramatically.

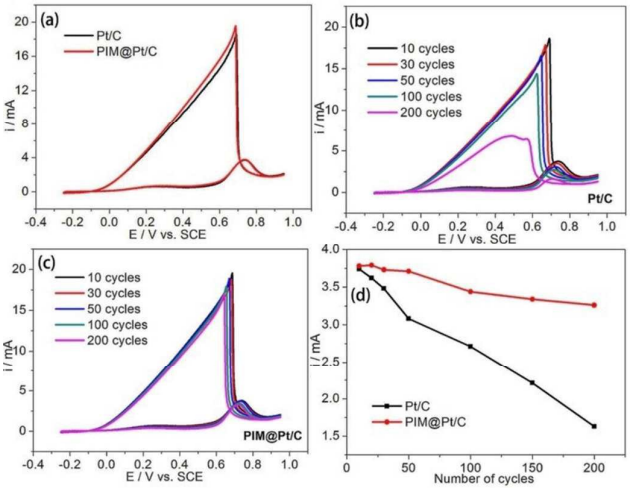

Fig. 4 (a) Cyclic voltammograms for formic acid oxidation at room temperature in a 0.1 M $HClO_4$ + 1 M HCOOH (50 mVs^{-1}). (b,c) Cyclic voltammograms for Pt/C (c) and for PIM@Pt/C (d) for accelerated degradation testing by potential cycling from -0.25 to +0.95 V vs. SCE. (d) Plot of oxidation peak currents for Pt/C and for PIM@Pt/C for the forward peak for formic acid electro-oxidation over 200 cycles.

RSC Advances Accepted Manuscript

The result for the forward scan oxidation peak currents versus number of potential cycles for both Pt/C and PIM@Pt/C are shown in Figure 4d. After 200 potential cycles, 85% of the initial forward oxidation peak current was still maintained for PIM@Pt/C, whereas only 43% activity remained for Pt/C. This again demonstrates enhanced durability during accelerated degradation testing when the PIM-EA-TB coating is applied to the catalyst.

Conclusions

A significant improvement in catalyst durability and performance (under accelerated degradation conditions) has been achieved by applying a PIM-EA-TB film as protective over-coating to commercial fuel cell anode catalyst materials. It is suggested that the molecularly rigid and microporous nature of the PIM-EA-TB material are crucial in (i) mechanically stabilizing both carbon substrate and platinum nano-catalyst, (ii) preventing electrophoretic mobility, (iii) not directly interacting with the platinum nano-catalyst surface sites, whilst (iv) preventing larger adsorbates reaching the catalyst surface. Enhanced stability does not come at the cost of reduced performance as the flow of reagents and charges through the microporous PIM-EA-TB environment is sufficient for good catalysis. Materials properties at the molecular level are important for catalyst performance improvement for a range of potential fuel cell technologies (and beyond). We believe our methodology provides a new and general route to increase fuel cell anode catalyst performance and lifetime.

Experiment section

Chemical Reagents

Commercial Pt/C (40 wt. % on Vulcan-72) catalysts and Nafion (5 wt. %) were obtained from Johnson Matthey and Dupont, respectively. Isopropanol, chloroform, and perchloric acid (70%–72%), were purchased from Aldrich or Fisher Scientific and used without further purification. PIM-EA-TB was prepared following a literature recipe.[36] Solutions were prepared with filtered and deionized water of resistivity 18.2 MW cm from a Thermo Scientific water purification system (ELGA).

Instrumentation and Procedures

Electrochemical measurements were performed with a μAutolab III system in a conventional three electrode cell with KCl-saturated calomel (SCE) reference and platinum wire counter electrode. A Pine AFMSRCE electrode rotator was used for rotating disk electrode (RDE) experiments. Data obtained in stationary solution and with rotation were essentially identical and therefore only stationary experiments are reported here. Morphologies of the prepared catalysts were analyzed with a JEOL FESEM 6301F scanning electron microscopy (SEM) and a JEOL 2010 high-resolution transmission electron microscope (HRTEM).

Procedures for electrode preparation

2 mg of Pt/C catalyst and 100 μL of 5 wt. % Nafion solution were dispersed in 1 mL of isopropanol, followed by a sonication for at least 15 min to form a homogeneous catalyst ink. A volume of 8 μL of the ink was loaded onto a glassy carbon (GC) disk electrode with a diameter of 6 mm. The catalyst layer was allowed to dry under ambient conditions before a CV measurement. Polymer with Intrinsic Microporosity Coating Pt/C (PIM@Pt/C) was conducted as follow: a solution of 1 mg cm^{-3} PIM-EA-TB was prepared in chloroform and 10 μL was applied directly by coating the Pt/C catalyst layer followed by drying under ambient conditions.

Acknowledgements

D.H. thanks the Royal Society for a Newton International Fellow. F.M. and N.M. thank the Leverhulme Trust for support (RPG-2014-308). F.M. thanks Dr. Robert Potter from Johnson–Matthey for support with catalyst materials and for helpful discussion.

References

1 H. Liu, C. Song, L. Zhang, J. Zhang, H. Wang, P. Wilkinson, *J. Power Sources,* 2006, **155**, 95.
2 S. K. Kamarudin, F. Achmad and W. R. W. Daud, *Int. J. Hydrogen Energy,* 2009, **34**, 6902.
3 M. Z. F. Kamarudin, S. K. Kamarudin, M. S. Masdar and W. R. W. Daud, *Int. J. Hydrogen Energy,* 2013, **38**, 9438.
4 X. Yu and P. G. Pickup, *J. Power Sources,* 2008, **182**, 124.
5 J. Park, H. Oh, T. Ha, Y.I. Lee and K. Min, *Applied Energy*, 2015, **155**, 866.
6 L. Li, L.P. Hu, J. Li and Z.D. Wei, *Nano Res*., 2015, **8**, 418.
7 X. Zhao, M. Yin, L. Ma, L. Liang, C. P. Liu, J. H. Liao, T. H, Lu and W. Xing, *Energ. Environ. Sci*., 2011, **4**, 2736.
8 F. Vigier, C. Coutanceau, A. Perrard, E.M. Belgsir and C. Lamy, *J. Appl. Electrochem.*, 2004, **34**, 439.
9 C. Rice, S. Ha, R. I. Masel and A. Wieckowski, *J. Power Sources,* 2003, **115**, 229.
10 N. C. Cheng, M. N. Banis, J. Liu, A. Riese, X. Li, R. Y. Li, S. Y. Ye, S. Knights and X. L. Sun, *Adv. Mater*., 2015, **27**, 277.
11 N. C. Cheng, M. N. Banis, J. Liu, A. Riese, S.C. Mu, R.Y. Li, T. K. Sham and X. L. Sun, *Energ. Environ. Sci*., 2015, **8**, 1450.
12 E.G. Ciapina, S. F. Santos and E. R. Gonzalez, *J. Electroanal. Chem.,* 2010, **644**, 132.
S. Chen, Z. Wei, X. Qi, L. Dong, Y. Guo, L.Wan, Z. Shao and L. Li, *J. Am. Chem. Soc.,* 2012, **134**, 13252.
13 M. W. Breiter *J. Electroanal. Chem. Interfacial Electrochem.*, 1967, **15**, 221.
14 M. Zhiani, B. Rezaei and J. Jalili, *Int. J. Hydrogen Energy,* 2010, **35**, 9298.
15 D. P. He, C. Zeng, C. Xu, N. C. Cheng, H. G, Li, S. C. Mu and M. Pan, *Langmuir,* 2011, **27**, 5582.
16 M. Zhiani, B. Rezaei, and J. Jalili, *Int. J. Hydrogen Energy*, 2010, **35**, 9298.
17 D. P. He, S. C. Mu and M. Pan, *Carbon,* 2011, **49**, 82.
18 D. P. He, K. Cheng, H. G. Li, T. Peng, F. Xu, S. C. Mu and M. Pan, *Langmuir,* 2012, **28**, 3979.
19 Z. Q. Tian, S. P. Jiang, Z. Liu and L. Li, *Electrochem. Commun.* 2007, **9**, 1613.
20 N. B. McKeown and P. M. Budd, *Macromolecules*, 2010, **43**, 5163.
21 T. Fujigaya, M. Okamoto, K. Matsumoto, K. Kaneko and N. Nakashima, *ChemCatChem*, **2013**, *5*, 1701.
22 N. B. McKeown, B. Gahnem, K. J. Msayib, P. M. Budd, C. E.Tattershall, K. Mahmood, S. Tan, D. Book, H. W. Langmi and A. Walton, *Angew. Chem. Int. Ed.* 2006, **45**, 1804.

RSC Advances Accepted Manuscript

This journal is © The Royal Society of Chemistry 20xx

23 C. G. Bezzu, M. Carta, A. Tonkins, J. C. Jansen, P. Bernardo, F. Bazzarelli and N. B. McKeown, *Adv. Mater.* 2012, **24**, 5930
24 S. V. Adymkanov, Y. P. Yampolskii, A. M. Polyakov, P. M. Budd, K. J. Reynolds, N. B. McKeown and K. J. Msayib, *Polymer Sci*. 2008, **50**, 444.
25 P. M. Budd, N. B. McKeown, B. S. Ghanem, K. J. Msayib, D.Fritsch, L. Starannikova, N. Belov, O. Sanfirova, Y. P. Yampolskii and V. Shantarovich, *J. Membrane Sci*. 2008, **325**, 851.
26 E. Madrid, Y. Rong, M. Carta, N.B. McKeown, R.M. Evans, G.A. Attard, T.J. Clarke, S.H. Taylor, Y. Long and F. Marken, *Angew. Chem*. 2014, **40**, 10927.
27 E. Madrid, P. Cottis, Yuanyang Rong, Adrian T. Rogers, J. M. Stone, R. Malpass-Evans, M. Carta, N. B. McKeown and F. Marken, *J. Mater. Chem. A,* 2015, **3**, 15849.
28 F. J. Xia, M. Pan, S. C. Mu; R. Malpass-Evans, M. Carta, N. B. McKeown, G. A. Attard, A. Brew, D. J. Morgan and F. Marken, *Electrochim. Acta*, 2014. **46**. 26.
29 Y. Y. Rong, R. M. Evans, M. Carta, N. B. McKeown, G. A. Attard and F. Marken, *Electroanalysis*, 2014, **26**, 904.
30 Y. Y. Rong, R. M. Evans, M. Carta, N. B. McKeown, G. A. Attard and F. Marken, *Electrochem. Commun*. 2014, **46**, 26.
31 D. P. He, Y. Y. Rong, Z. K. Kou, S. C. Mu, T. Peng, R. Malpass Evans, M. Carta, N. B. McKeown and F. Marken, *Electrochem. Commun*. 2015, **59**, 72.
32 C.E. Hotchen, G.A. Attard, S.D. Bull, and F. Marken, *Electrochim. Acta,* 2014, **137**, 484.
33 S. Wasmus and A. Kuver, *J. Electroanal. Chem*. 1999, **461**, 14.
34 Z.Y. Zhou, Z.Z. Huang, D.J. Chen, Q. Wang, N. Tian, and S.G. Sun, *Angew. Chem. Int. Ed*. 2010, **49**, 411.
35 X.W. Yu, and P.G. Pickup, *J. Power Sources*, 2008, **182**, 124.
36 M. Carta, R. Malpass-Evans, M. Croad, Y. Rogan, J. C. Jansen, P. Bernardo, F. Bazzarelli, N. B. McKeown, *Science*, 2013, **339**, 303.

Graphical Abstract

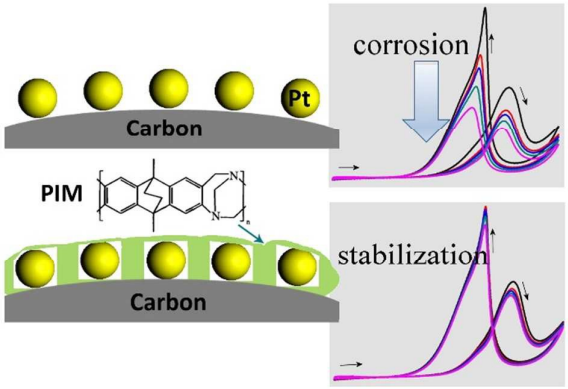

RSC Advances Accepted Manuscript